Macromolecules

ARTICLE

pubs.acs.org/Macromolecules

Interactions of Biological Buffers with Macromolecules: The Ubiquitous "Smart" Polymer PNIPAM and the Biological Buffers MES, MOPS, and MOPSO

Mohamed Taha, Bhupender S. Gupta, Ianatul Khoiroh, and Ming-Jer Lee*

Department of Chemical Engineering, National Taiwan University of Science and Technology, 43 Keelung Road, Section 4, Taipei 106-07, Taiwan

ABSTRACT: Proteins are practically never in a buffer-free solution. We therefore studied the effects of some important biological buffers 2-(*N*-morpholino)ethanesulfonic acid (MES), 3-(*N*-morpholino)propanesulfonic acid (MOPS), and 3-morpholino-2-hydroxypropanesulfonic acid (MOPSO) on the lower critical solution temperature (LCST) phase transition of poly(*N*-isopropylacrylamide) (PNIPAM), an isomer of polyleucine, as a model compound for protein. The results from dynamic light scattering (DLS) analysis showed that the LCST of PNIPAM aqueous solutions were decreased significantly with increasing the buffer concentration, due to the presence of the buffers destroying the hydration structures and subsequent aggregation of PNIPAM. Based on density functional theory (DFT) and molecular mechanics calculations, these buffers are highly polar compounds and, therefore, strongly interact with water molecules, causing buffering out of PNIPAM. The buffer's affinity to water follows the order MOPS > MES > MOPSO. The LCST values determined from DLS follow the order MOPSO > MOPS ≈ MES. The Fourier transform infrared spectra (FTIR) reveal that no direct binding between the buffer and the polymer occurs but interacts with the first hydration shell of the polymer. In comparing with the MOPS buffer, the unexpected effects on the PNIPAM were found in the MOPSO-containing system due to MOPSO has one more OH group. This group interacts with water clusters around the hydrophobic isopropyl groups, which changes the hydration state of the polymer. It also should be noted that the phase transition in the presence of buffers is similar to those observed with kosmotropic salts and sugars (protein stabilizers) in terms of lowering the LCST and the dehydration of PNIPAM groups. Such favoring of the compact globule state observed at high buffer concentrations will provide a protective effect against denaturation of globular proteins. The interactions of the studied buffers with bovine serum albumin (BSA) have been investigated and found that these buffers stabilized BSA, based on DLS, FTIR, and UV−vis absorption studies. The present study will act as a key for the lock of buffer and macromolecule mechanism.

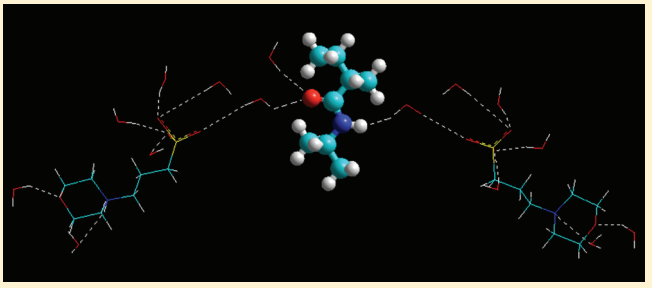

1. INTRODUCTION

Proteins are generally linear polymers of many amino acids, and thereby polyamides. The amide linkage is often called a peptide bond, and proteins are polypeptides. Macromolecules such as proteins need a distinct three-dimensional structure within the aqueous surrounding to perform specific functions. As we all know, stability of proteins is important in various fields such as biochemistry, medicine, pharmacy, and industry. Proteins are often unstable and denatured when not in their native environments. The interactions of protein with its surrounding medium (solvent) play a central role in its stability in aqueous solution. Most of these interactions are nonbonded such as hydrogen bonding, electrostatic, and hydrophobic interactions. Usually, proteins must be investigated in buffered solutions to keep the pH of the solution constant and the protein in a defined protonation state. Otherwise, the change in the pH of the solution may have a significant influence on the protein stability. In some cases, where the protein concentration is relatively high, the protein rather the buffer, supplies the majority of the buffering capacity.

Most of the biological buffers used today were developed by Good and co-workers.[1,2] These organic buffers are N-substituted taurine or glycine derivatives, which provide good coverage of the physiological pH range (6.1−10.4). These buffers are frequently called Good's buffers, and their acronyms are spread throughout the biochemical literature and laboratory manuals. These Good buffers are now widely used throughout the world, since they meet most of the requirements that biological buffers have to fulfill. Ideally, the buffers should be inert, but it seems they are not as inert as originally believed. Therefore, the selections of a proper buffer will always depend on extensive testing.[3]

Despite much work on the study of proteins in buffer solutions, no mechanism has been able to satisfactorily explain the stabilization/destabilization properties of the proteins in buffer solutions. The same buffers can be either stabilize or

Received: August 4, 2011
Revised: September 28, 2011
Published: October 18, 2011

destabilize different proteins. Also, the same proteins may be stabilized and destabilized by different buffers. It is considered that if a certain buffer can bind selectively to native state of a protein, it would increase the protein stability. On the other hand, when a buffer binds preferentially to the denatured state, it decreases its stability. Other studies, however, have suggested that some buffers can act as efficient radical scavengers.[4−7]

The selected biological buffers 2-(*N*-morpholino)ethanesulfonic acid (MES), 3-(*N*-morpholino)propanesulfonic acid (MOPS), and 3-morpholino-2-hydroxypropanesulfonic acid (MOPSO) have aqueous pK_a values covering the pH range from 5.5 to 7.9. These buffers are structurally related compounds, each one containing a morpholine ring.[8] Up to date, MES and MOPS are the most widely used in various biological and biochemical studies due to their presumably more inert properties.[9] The Good buffer based on the morpholine ring, MES, is suitable for the investigation of redox processes. Since MES does not form any radicals in the presence of H_2O_2, oxygen radicals, or autoxidizing iron or under certain electrolytic conditions. In contrast to this, radical species are formed from the piperazine ring-based buffers HEPES (4-(2-hydroxyethyl)piperazine-1-ethanesulfonic acid), HEPPS (4-(2-hydroxyethyl)-1-piperazinepropanesulfonic acid), and PIPES (1, 4-piperazinediethanesulfonic acid).[8] Both morpholine ring-containing buffers (MES and MOPS) and piperazine ring-containing zwitterionic buffers (HEPES, HEPPS, and PIPES) are oxidized by H_2O_2 to their N-oxide forms, but the rate of oxidation is slow in the case of MOPS buffer. Different protein aggregation behavior has been observed within various buffer species at the same pH value. For instance, lower aggregation propensity of humanized antibody by MES and MOPS buffers than by phosphate and citrate buffers has been reported.[10] The activity of endo-α-D-mannosidase enzyme in MES and MOPSO buffers at pH 7.0 is increased very much over buffers like HEPES or HEPPS and was essentially eliminated in the presence of TRIS buffer.[11] Assembly of bovine brain protein in MES showed a higher recovery microtubule protein when compared with PIPES buffer.[12] MES and MOPS were the only buffers tested among several zwitterionic buffers that had a negligible effect in the bicinchoninic acid (BCA) protein assays.[13] Use of MOPS buffer favors synthesis of noncrystalline and crystalline cellulose over callose (β-1,3-glucan).[14] The interactions between the zwitterionic buffers MOPS, HEPES, or TES with DNA transcription in bovine embryos at pH 7.2 showed the advantage of MOPS over remaining tested buffers.[15] MOPSO has been employed as a buffer component of charcoal yeast extract medium.[16] The interactions of DNA with various neutral pH, amine-based buffers have been investigated.[17] The results indicate that DNA−buffer interactions are very common, especially in neutral pH, amine-based buffers.[17]

MES is a popular buffer used in protein crystallization. At present, several hundred structures in the Protein Data Bank (PDB) contain ordered MES, revealing that it is common to have specific interactions between buffers and protein molecules.[18] The PDB contains several crystallized proteins, which have been found to form complexes with MES buffer. MES was found to form a complex with metallo-β-lactamase enzyme (from *Bacteriodes frgilis*).[19] In that complex, two of the oxygen atoms of the sulfonic acid group of MES form hydrogen bonds with Wat 254, and the third sulfonic acid oxygen forms a hydrogen bond with the amide nitrogen of Asn 176. In the second example, the sulfonic acid moiety of MES binds in a phosphate binding site in the structure of indole-3-glycerol phosphate synthase from *Solfulobus solfataricus*.[20] One more example, MES, was found in the active site of dialkyl decarboxylase, next to the position of the bound pyridoxyl-5′-phosphate cofactor.[21] The MES buffer interference with human liver fatty acid binding protein (hLFABP) dynamics on a microsecond to millisecond time scale in aqueous solution has been reported.[22]

Proteins consist of a wide range of active functional groups attached to the side chains of their polypeptide backbone, which are capable of interacting with solvent molecules. Because the peptide backbone is the most abundant group in a protein, it makes a particularly useful factor in studying protein−solvent interactions. Therefore, it would be of interest to investigate the interactions between the peptide group and buffer molecules, rather than to deal with the protein as a whole. For this purpose, we selected a simple polymer model, poly(*N*-isopropylacrylamide) (PNIPAM), in place of a protein. PNIPAM is an isomer of poly(leucine), but with a pendant peptide group in the side chain rather than in the backbone. As a consequence, the only interacting site of PNIPAM with buffer is the peptide group since this polymer does not contain any other hydrogen bond donating or accepting groups. Spectroscopic measurements using such a model are easier to interpret.

When an aqueous solution of PNIPAM is heated above ca. 32−35 °C (the low critical solution temperature, LCST, or cloud point, CP), the polymer molecules undergo phase transition from random coil form into compact globule form. However, at the same time, aggregation of the globules will occur to give an optically detectable phase transition, and in the cooling process the phase transition can be recovered easily to its original state. The reason that we selected the PNIPAM polymer is not really the fact that its LCST is close to body temperature (other polymers exhibit LCST values even closer to 37 °C) but rather the fact that PNIPAM shows unique sensitivity to environmental conditions such as pH,[23] ionic strength,[24] pressure,[25] etc. This behavior has attracted considerable attention because of a certain similarity for many biological systems, such as protein folding, native DNA packing, and network collapsing.[26] The transition from a coil to a globule has been related to the competitive results of two types of intermolecular forces: the hydrophobic interaction of pendent isopropyl groups and backbones and the hydrogen bonding between amide groups and water molecules,[27−33] Plenty of investigations have been devoted to elucidate the effects of salts,[34−37] cosolvents,[38−59] surfactants,[60−64] urea,[65] sugars,[66] and ionic liquids[67] on the phase transition of PNIPAM in aqueous medium. Indeed, studies on phase transition behavior of PNIAM are very helpful to understand the nature of the interactions between solvents and proteins.

The main objective of the present work was to study the interactions of widely used biological buffers (MES, MOPS, and MOPSO) with the amide moiety of PNIPAM, as a model providing certain key behavior of protein−buffer interactions. For this purpose, we studied the LCST of PNIPAM in the presence of increasing buffer concentrations by means of dynamic light scattering (DLS) and Fourier transform infrared (FTIR) spectroscopy techniques. Another important opportunity is to explore LCST behavior of PNIPAM in the presence of buffers. From the technological point of view, PNIPAM has potential applications include drug or dye delivery,[68,69] tissue engineering,[70] templates for nanoparticles,[71] biosensing,[72] and catalysis,[73] just to enumerate a few. To explore the effect of these buffers on a protein, we have selected bovine serum albumin (BSA) protein for our experimental validation. BSA is selected as our protein model because of its many applications, both in

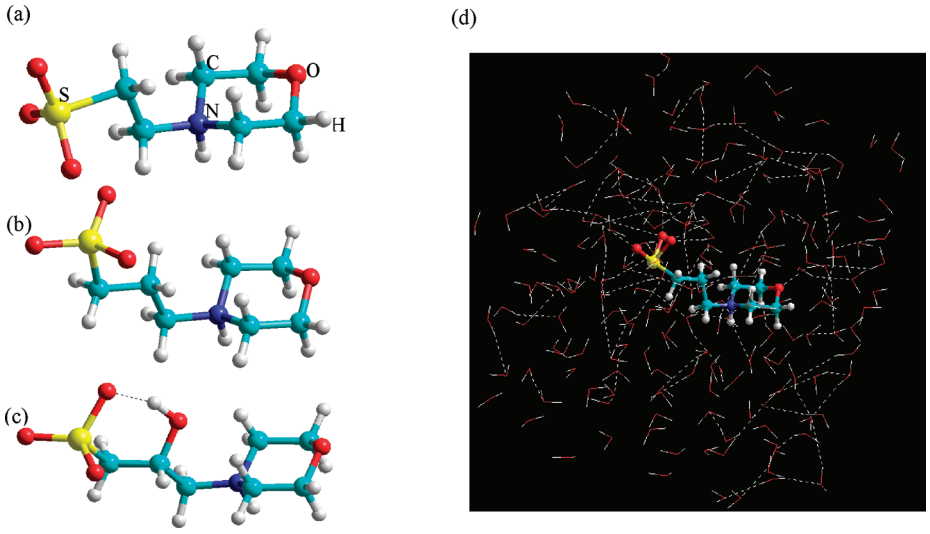

Figure 1. Optimized structures obtained by DFT at the B3LYP/6-31G level of the zwitterionic buffers (a) MES (b) MOPS, and (c) MOPSO in gas phase; (d) MOPS buffer inside an aqueous solution under PBC.

clinical medicine and in basic research. BSA is a single polypeptide chain of molecular weight 66 kDa with 583 amino acid residues. The general folding nature of this protein polypeptide is strongly restricted by 17 disulfide bridges. Albumin is the most abundant soluble protein in the body of all vertebrates and is the most plasma protein in the blood.[74]

2. EXPERIMENTAL SECTION

Materials. PNIPAM (M_n = 20 000−25 000) and the buffers, MES (mass fraction purity >0.99), MOPS (mass fraction purity >0.995), and MOPSO (mass fraction purity >0.99), were purchased from Sigma Chemical Co. All of the received materials were used without further purification. Water used for preparing aqueous solutions was obtained from NANO pure-Ultra pure water system that was distilled and deionized with resistivity of 18.3 MΩ cm. BSA/fraction V, pH = 7.0, and deuterium oxide (D_2O, mass fraction purity = 0.998 atom D) were obtained from Acros Organics. All samples were prepared gravimetrically using an electronic balance (R&D, Model GR-200) with a precision of ±0.1 mg.

Methods. The hydrodynamic diameter (d_H) was estimated with a Zetasizer Nano ZS90 (Malvern Instruments Ltd., UK) using dynamic light scattering. The light source of the instrument is a 4 mW He−Ne laser with a fixed wavelength, λ = 633 nm. The instrument measures the time-dependent fluctuation in the intensity of the light scattered from the particles in solution at a fixed scattering angle 90°. Thus, the hydrodynamic diameter obtained was an apparent *z*-averaged hydrodynamic diameter. The scattering intensity data were processed using the instrumental software to obtain the averaged hydrodynamic diameter (d_H) and the size distribution. The value of d_H was obtained from the Stokes−Einstein equation defined as

$$d_H = \frac{kT}{3\pi\eta D} \quad (1)$$

where k is the Boltzmann's constant ($1.3806503 \times 10^{-23}$ m^2 kg s^{-2} K^{-1}), T is absolute temperature (K), η is viscosity (mPa s), and D is diffusion coefficient (m^2 s^{-1}). The instrument is equipped with a thermostatic sample chamber for maintaining the desired temperatures within a temperature range of 0−90 °C. A bubble free sample of around 1.5 cm^3 was introduced in a square glass cuvette with round aperture (PCS8501) sample cell through a syringe. A Teflon-coated screw cap was placed at the mouth of cell to secure from dust. Then the airtight sample cell was placed in the sample chamber of DLS instrument. In the heating scans, the temperature was scanned between 10 and 45 °C, and three measurements were performed at each temperature. The time for one total heating cycle between 10 and 45 °C was between 8 and 12 h. The samples for DLS analysis were prepared with 6 mg cm^{-3} of PNIPAM and varying the concentrations of buffer from 0.0 to 0.9 M. The samples for BSA were prepared with 20 mg cm^{-3} in 0.05, 0.2, and 1.0 M H_2O buffer at pH = 7.0.

The Fourier transform infrared spectra were obtained by using a Bio-Rad Digilab FTS-3500 spectrometer. The PNIPAM/BSA samples dissolved in solvent (water buffer/D_2O buffer) were placed between two ZnSe windows (32 mm diameter, Sigma-Aldrich) and a spacer (0.015 mm thick, EZ copper). The IR cell was attached to a metal cell holder and equipped with a controlled temperature cell (Model HT-32 heated transmission cell). Each IR spectrum reported here was an average of 200 scans using a spectral resolution of 8 cm^{-1}. Analyses of the spectra were performed by using spectroscopic software (Varian Resolutions, Version 4.10). A background spectrum of the solvent was measured directly before each sample containing PNIPAM. The samples for FTIR spectroscopy were prepared with 20 mg cm^{-3} of PNIPAM in 0.0−0.9 M water buffer or in 0.0, 0.3, and 0.7 M D_2O buffer. The samples for BSA were prepared with 30 mg cm^{-3} in 0.05 and 1.0 M D_2O buffer (MES, MOPS, or MOPSO) at pD = 7.4. The pD value of the BSA solution was measured with a HTC-210U pH meter using glass electrode, and the value was corrected according to pD = pH + 0.4 for deuterium isotope effects. The pH-meter was calibrated before each titration with pH 4.0 and 7.0 standard buffer solutions.

The UV−vis spectra were recorded for 2.5 mg cm^{-3} of BSA in 0.05, 0.2, 0.5, and 1.0 M buffer solutions at room temperature on a V-550 spectrophotometer (JASCO) equipped with 1.0 cm quartz cells.

Computational Details. The optimized geometries of the zwitterionic buffers MES, MOPS, and MOPSO involving density functional theory (DFT) and molecular mechanics methods were performed by using the molecular modeling program HyperChem 8.0.7.[75] The dipole moment of the studied buffers has been calculated in gas phase and aqueous solution. In the gas phase, the dipole moment and the total energy of the zwitterionic buffers were calculated by using DFT-SCF at Hartree−Fock (HF)/B3LYP levels with the standard 6-31G basis set, and the optimized geometries are shown in Figure 1a−c. The optimized geometries of the zwitterions by DFT calculations then placed inside an

aqueous solution under a periodic boundary condition (PBC) of dimension 18.7 × 18.7 × 18.7 Å ($x-y-z$) and containing 216 randomly distributed water molecules to simulate an aqueous environment (Figure 2d, as a representative). A minimum distance between the solutes and the water molecules of 2.3 Å was used to ensure a weak force-field environment. Then, the system was optimized by molecular mechanics, with an AMBER 3 force field and Polak-Ribiere conjugate gradient optimizer. All water molecules are explicitly included in the calculation and described with the TIP3P model.[76] The resulting zwitterions' structure followed by a single-point energy calculation, using DFT at the B3LYP/6-31G level.

3. RESULTS AND DISCUSSION

In order to monitoring the LCST of PINIPAM in water and in aqueous buffer solutions, the DLS measurements were conducted through heating from 10 to 45 °C. The temperatures scan of the sample enables examination of both size and the intensity distribution graph with their respective temperatures. In addition, DLS is a powerful tool to get detail information about the size distribution of the aggregates. The LCST values were obtained by plotting the averaged hydrodynamic diameter (d_H) of PINPAM in aqueous solution with and without buffer as a function of temperature. The results of our DLS investigations are listed in Tables 1−3. Figure 2a−c shows the values of d_H as a function of temperature for PNIPAM in 0, 0.1, 0.3, 0.5, 0.7, and 0.9 M buffer solutions. Below LCST, Figure 2 shows that the d_H of PNIPAM in pure water was very slightly changed (15.8−18.1 nm) from 10 to 33 °C for PNIPAM. This indicates that the PNIPAM in coil conformation due to the hydrogen bonding between amide groups (CONH) of polymer and water molecules. When temperature reaches about 34 °C, PNIPAM in water is fully collapsed and starts the globule state because d_H rapidly increased to 570 nm. This indicates that the phase transition of PNIPAM in water occurs at 34 °C. The d_H values gradually decrease to an almost constant value (∼75 nm) when the temperature of aqueous PNIPAM solution is raised above the LCST (34 °C). In the globule state, aggregation occurs due to the hydrophobic interactions among hydrophobic groups located on the surface of the collapsed polymer. Since the majority of the hydrogen bonds between the amide groups and water molecules are ruptured. As a result, most of the amide groups being buried inside the globules, by forming H-bonds between them. Clearly, if these amide groups H-bonded with water, a large amount of water molecules would cover the globule surface, therefore preventing the aggregation. Indeed, the globule state of PNIPAM resembles to the native structure of globular protein, in which most of the peptide groups are buried in the interior.

The LCST values for PNIPAM were measured in 0.1, 0.3, 0.5, 0.7, and 0.9 M buffers (MES, MOPS, or MOPSO). It is clearly seen from Figure 2 that the dramatic decrease in the LCST of PNIPAM with increasing buffer concentrations reflects the enhancement of the collapsed state. Specifically, buffer decreases the LCST value from 34 °C (buffer free) to 33, 31, 29, 27, and 25 °C for MES, 33, 31, 29, 27, and 24 °C for MOPS, and 33, 31, 28, 25, and 21 °C for MOPSO in the presence of 0.1, 0.3, 0.5, 0.7, and 0.9 M buffer, respectively. The effect of MES, MOPS, and MOPSO buffers on the phase transition of PNIPAM is same at 0.1 and 0.3 M buffer, while at buffer concentrations greater than 0.3 M, the order of effectiveness in lowering the LCST values was MOPSO > MOPS ≈ MES. Through this, we can see that the buffer molecules reduce the water−polymer interactions. This

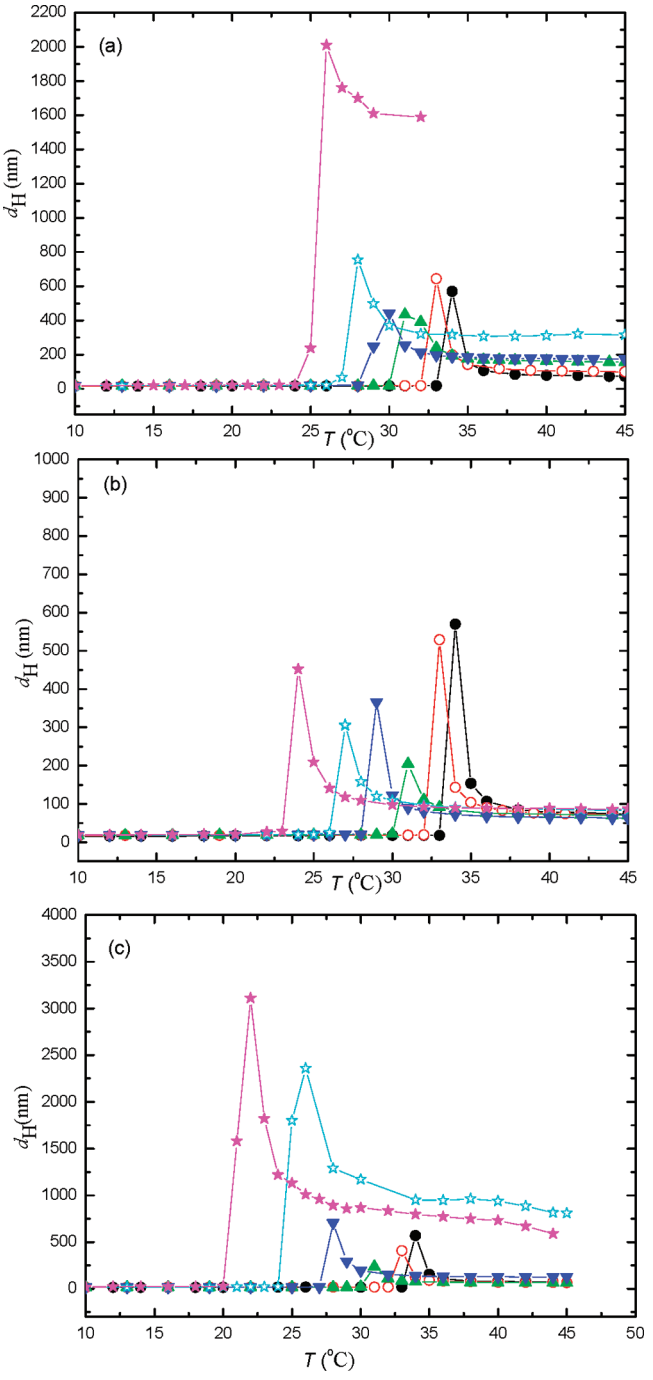

Figure 2. Hydrodynamic diameter (d_H) obtained from the intensity distribution graph as a function of temperature for PNIPAM in 0, 0.1, 0.3, 0.5, 0.7, and 0.9 M MES (a), MOPS (b), or MOPSO (c) as a function of temperature: 0.0 M (●), 0.1 M (○), 0.3 M (▲), 0.5 M (▼), 0.7 M (☆), and 0.9 M (★).

decrease in the phase transition of PNIPAM represents the buffering-out effect caused by the buffer. The same behavior was observed previously for PNIPAM in aqueous solutions of soluting-out agents such as kosmotropic ions and sugars.[24] Kosmotropic ions (strongly hydrated ions) show stronger attraction with water molecules compared with water−water interactions; thus, they organize several layers of water molecules around themselves. The kosmotropic anions were found to

Table 1. DLS Data of Hydrodynamic Diameter (d_H) for PNIPAM in 0, 0.1, 0.3, 0.5, 0.7, and 0.9 M MES Buffer Solutions at Different Temperatures

water		0.1 M MES		0.3 M MES		0.5 M MES		0.7 M MES		0.9 M MES	
T (°C)	d_H (nm)	T (°C)	d_H (nm)	T (°C)	d_H (nm)	T (°C)	d_H (nm)	T (°C)	d_H (nm)	T (°C)	d_H (nm)
10	15.8	10	17.1	10	18.1	10	18.4	10	18.7	10	19.5
12	15.8	13	17.4	13	18.1	13	18.5	13	18.7	12	19.5
14	16.0	16	17.5	16	18.2	16	18.9	16	18.7	14	20.1
16	16.2	19	17.9	19	18.3	19	19.1	19	19.2	15	20.4
18	16.4	22	17.9	22	18.8	22	19.4	22	19.7	16	20.4
20	17.1	25	18.0	25	18.9	25	19.8	25	20.7	17	20.6
22	17.1	28	18.4	28	19.4	28	20.7	26	20.8	18	20.7
24	17.3	31	18.5	29	19.6	29	248.0	27	67.8	19	21.2
26	17.6	32	19.2	29	19.7	30	443.0	28	755.0	20	21.1
28	17.6	33	644.0	30	20.1	31	255.0	29	498.0	21	21.5
30	17.7	34	200.0	31	434.0	32	214.0	30	369.0	22	21.8
31	17.7	35	143.0	32	391.0	33	197.0	32	321.0	23	23.1
32	18.0	37	118.0	33	239.0	34	188.0	34	317.0	24	24.0
33	18.1	39	109.0	34	195.0	35	185.0	36	307.0	25	238.0
34	570.0	41	104.0	35	178.0	36	182.0	38	309.0	26	2010.0
35	154.0	43	103.0	36	171.0	37	179.0	40	311.0	27	1760.0
36	107.0	45	100.0	37	170.0	38	178.0	42	321.0	28	1700.0
38	84.6			38	167.0	39	179.0	45	316.0	29	1610.0
40	78.8			40	164.0	40	178.0			32	1590.0
42	77.4			42	159.0	41	174.0				
44	74.5			44	158.0	42	175.0				
45	73.2			45	157.0	43	175.0				
						45	175.0				

polarize water molecules that were directly hydrogen bonded with the amide moieties of PNIPAM.[24] Most sugars are known to act as kosmotropic substances[77] and protein structure stabilizers. The protein stabilization by sugars has been explained to be due to the preferential exclusion of the sugars from the protein vicinity leading to preferential hydration of the protein.[78,79] Kosmotropic salts tend to precipitate proteins from solution and provide protection to proteins. The solubilities of MES, MOPS, and MOPSO buffers in water and aqueous solutions of ethanol or 1,4-dioxane have been recently studied by us at 298.15 K.[80,81] We found that these buffers are highly soluble in water and practically insoluble in organic solvents. The solubilties of these buffers in water are 28.8, 155.2, and 89.1 g/100 g of water for MES, MOPS, and MOPSO, respectively. The unexpected low solubility of MOPSO than that of MOPS is due to that the hydroxyl group of MOPSO forms intrahydrogen bond with the zwitterions. The optimization geometry of MOPSO molecules obtained from DFT at the B3LYP/6-31G level shows the intrahydrogen bond between the hydroxyl group and the sulfonic group as shown in Figure 1c. Interestingly, MOPS buffer was able to exclude 1,4-dioxane from it aqueous solutions to form a new liquid phase, and the phase separation was observed over a given composition range at ambient conditions.[81] This is due to the high affinity of MOPS with water molecules comparing with water−organic solvent interactions. The zwitterions, like salts, have very large dipole moments,[82−84] which make them interact strongly with water molecules. The dipole moments of MES, MOPS, and MOPO are not experimentally measured. However, it is possible to calculate the dipole moment of these compounds from quantum calculations. Here, we try to calculate their dipole moments using DFT at the B3LYP/6-31G level. We calculated the dipole moment of the zwitterionic buffer both in the gas phase and in aqueous solution under a periodic boundary condition. The calculated dipole moments (debye) obtained in gas phase are 18.67, 23.76, and 20.64 for MES, MOPS, and MOPSO, respectively, whereas the corresponding values obtained in aqueous solution under a periodic boundary condition are 22.99, 24.01, and 16.32 for MES, MOPS, and MOPSO buffers, respectively. Therefore, the high affinity of these buffers to water molecules is due to the high dipole moments of these molecules. It is thus suggested that these zwitterionic buffers are kosmotropic salt-like molecules and that should be due to their dipolar nature (zwitterions). From these results, it might be expected that these buffers would also stabilize proteins especially at high concentrations because we found recently that increasing the TRIS buffer concentration increased the thermal stability of bovine serum albumin (BSA) protein, based on a variety of biophysical measurements.[85]

Turning now to the DLS results, Figure 3 shows the intensity distribution graphs of PNIPAM in 0−0.9 M MES aqueous solutions, at different temperatures including their respective LCST values. For brevity's sake, the intensity distribution graphs for other buffers solutions are not shown. However, similar trends were found from other buffer systems (containing MOPS or MOPSO) as well. For PNIPAM in pure water, one peak was observed in the intensity distribution graph (Figure 3a) at 10 °C, corresponding to the effective diameter 15.8 nm. This indicates that all the PNIPAM

Table 2. DLS Data of Hydrodynamic Diameter (d_H) for PNIPAM in 0, 0.1, 0.3, 0.5, 0.7, and 0.9 M MOPS Buffer Solutions at Different Temperatures

water		0.1 M MOPS		0.3 M MOPS		0.5 M MOPS		0.7 M MOPS		0.9 M MOPS	
T (°C)	d_H (nm)	T (°C)	d_H (nm)	T (°C)	d_H (nm)	T (°C)	d_H (nm)	T (°C)	d_H (nm)	T (°C)	d_H (nm)
10	15.8	10	17.3	10	18.2	10	18.4	10	18.7	10	18.9
12	15.8	13	17.8	13	18.3	12	18.4	12	18.7	12	18.9
14	16.0	16	17.8	16	18.3	14	18.8	14	19.0	14	19.3
16	16.2	19	17.8	19	18.9	16	18.9	16	19.3	16	19.7
18	16.4	22	18.3	22	19.0	18	18.9	18	19.3	18	20.1
20	17.1	25	18.3	25	19.4	20	19.2	20	19.7	20	20.1
22	17.1	28	18.5	28	19.9	22	19.5	22	19.9	22	27.2
24	17.3	31	18.7	29	20.0	24	19.5	24	19.9	22	27.4
26	17.6	32	18.9	30	22.1	25	19.7	25	20.4	23	28.6
28	17.6	33	529.0	31	205.0	26	19.7	26	25.2	24	452.0
30	17.7	34	143.0	32	111.0	27	20.4	27	305.0	25	209.0
31	17.7	35	104.0	33	91.3	28	20.9	27	307.0	26	141.0
32	18.0	36	90.7	34	83.4	29	366.0	28	158.0	27	118.0
33	18.1	37	83.1	36	76.6	30	123.0	29	120.0	28	109.0
34	570.0	38	80.2	38	74.6	31	90.4	30	109.0	30	97.4
35	154.0	39	76.8	40	72.6	32	80.4	32	96.1	32	92.4
36	107.0	40	76.2	42	71.3	34	72.0	34	90.5	34	89.8
38	84.6	41	74.3	44	69.9	36	67.8	36	88.6	36	88.9
40	78.8	42	73.2	45	70.9	38	66.1	38	88.2	38	88.4
42	77.4	44	72.4			40	65.4	40	86.5	40	88.9
44	74.5					42	64.7	42	84.5	42	87.2
45	73.2					44	63.7	44	83.3	44	86.1
						45	62.8	45	84.0	45	87.2

molecules are in hydrated form. Increasing temperature up to 34 °C (LCST) resulted in the formation of aggregate, as indicated by one peak at 570 nm, and this aggregate was clearly visible to the naked eyes. This large aggregate suggested that the intermolecular cross-linking between the polymer chains is dominant. With a further increase in temperature, beyond the LCST, the intensity of the peak is increased and shifted to lower aggregate size (73.2 nm) at 45 °C. This shrinking in aggregate size implies that intrachain cross-linking becomes dominant. Similar behavior was observed for the aggregates of PNIPAM in 0.1−0.5 M MES with that in MES-free solution (Figure 3b−d). However, the d_H values of PNIPAM in MES solution below the LCST values are higher than those in aqueous solution, as given in Tables 1−3. The changes in the size particles arise from the influence of MES buffer on PNIPAM, since these measurements were made below the LCST. The size distribution curve (Figure 3e) for PNIPAM in 0.7 M MES at 10 °C shows two peaks. One of these two peaks was obtained from a major population (18.9 nm) of high intensity, whereas the other population (5160 nm) corresponds to a lower percentage of intensity. The presence of the peak with a higher hydrodynamic diameter 5160 nm, showing that PNIPAM starts to collapse and aggregate at higher buffer concentrations even at lower temperatures. We should note in interpreting the intensity distribution graph that the area for high aggregation peak will appear at least 10^6 times larger than of the first peak for the smaller particles. This is because large particles scatter much more light than small particles. From Rayleigh's approximation, the intensity of scattering of a particle is proportional to the sixth power of its diameter, and thus, the larger particles in the second population are small. With increasing temperature to the transition temperature (27 °C), the intensity of the hydrated peak was decreased, and its size increased to 21.0 nm. While the intensity of the aggregated peak was increased, its size becomes more compacted (175.0 nm). Further increase in temperature, beyond the transition temperature, only one peak was observed at 45 °C with size 316 nm.

It was observed that the studied buffers aggregate at higher concentrations in pure water; i.e., MES buffer at 0.9 M has one peak at ∼1 nm. It is indicated that there is a strong buffer−buffer interaction at higher concentrations. The interactions between buffer molecules probably occur through hydrogen bonds, since each molecule has both hydrogen bond donor and acceptor atoms. The same peak is also observed for the others two buffers in pure water at 0.7 and 0.9 M. This peak was again observed in PNIPAM−buffer solutions before the LCST values, i.e., for PNIPAM in 0.9 M MES and in 0.7 and 0.9 M MOPS/MOPSO, respectively.

The intensity distribution graphs of PNIPAM in 0.9 M MES (Figure 3f) shows three peaks at 10 °C with particles size ∼1, 22.2, and 243 nm. The first peak is due to MES buffer aggregates, while the two remaining peaks are due to PNIPAM aggregates. Upon heating of PNIPAM to its transition temperature (25 °C) in 0.9 M MES, a peak due to the formation of PNIPAM aggregates appears (238 nm). Heating above the transition temperature converts this peak in more aggregated state (1590 nm). The appearance of the peak at ∼1 nm of the aggregated buffer (at high concentrations)

Table 3. DLS data of Hydrodynamic Diameter (d_H) for PNIPAM in 0, 0.1, 0.3, 0.5, 0.7, and 0.9 M MOPSO Buffer Solutions at Different Temperatures

water		0.1 M MOPSO		0.3 M MOPSO		0.5 M MOPSO		0.7 M MOPSO		0.9 M MOPSO	
T (°C)	d_H (nm)	T (°C)	d_H (nm)	T (°C)	d_H (nm)	T (°C)	d_H (nm)	T (°C)	d_H (nm)	T (°C)	d_H (nm)
10	15.8	10	17.0	10	17.2	10	17.3	10	17.4	10	17.6
12	15.8	13	17.2	13	17.4	13	17.8	13	18.1	12	22.9
14	16.0	16	17.4	16	17.6	16	17.9	16	18.3	14	22.9
16	16.2	19	17.6	19	17.8	19	18.5	19	19.7	16	24.3
18	16.4	22	17.8	22	18.2	22	19.1	20	20.2	18	24.4
20	17.1	25	18.1	25	18.5	25	19.4	21	20.9	20	27.7
22	17.1	28	18.5	28	19.1	27	21.0	22	21.5	21	1580.0
24	17.3	31	18.8	29	19.6	28	707.0	23	21.4	22	3110.0
26	17.6	32	19.1	30	23.3	29	294.0	24	23.6	23	1820.0
28	17.6	33	409.0	31	238.0	30	196.0	25	1800.0	24	1220.0
30	17.7	34	125.0	32	110.0	32	154.0	26	2360.0	25	1130.0
31	17.7	35	92.3	33	87.5	34	138.0	28	1290.0	26	1010.0
32	18.0	36	83.6	34	78.7	36	133.0	30	1170.0	27	960.0
33	18.1	38	75.4	36	73.8	38	131.0	34	952.0	28	891.0
34	570.0	40	70.7	38	70.0	40	130.0	36	947.0	29	858.0
35	154.0	42	69.6	40	67.7	42	127.0	38	963.0	30	868.0
36	107.0	44	68.5	42	66.6	44	126.0	40	938.0	32	836.0
38	84.6	45	67.7	44	66.5	45	126.0	42	886.0	34	796.0
40	78.8			45	66.1			44	814.0	36	773.0
42	77.4							45	811.0	38	748.0
44	74.5									40	731.0
45	73.2									42	670.0
										44	590.0

again in the presence of PNIPAM is quite curious. This probably indicates that the buffer does not interact directly with PNIPAM.

It is important to emphasize whether or not the buffer molecules interact with PNIPAM. Therefore, we have now carried out FTIR spectroscopy analysis, which is a quite suitable technique for observing the hydration changes of PNIPAM in the presence of buffer. For the present study, we characterize the frequencies of the amide I and II bands. The amide I peak is mainly due to C═O stretching vibrations, whereas the amide II peak consists of a combination of N−H bending with C−H stretching vibrations. The amide I and II peaks provide important information concerning hydrogen bonding of the amide group.

Figure 4a−c plots IR spectra of amide I and II bands of PNIPAM in water−buffer systems (0−0.9 M) at 20 °C. From the figure, the amide I and II bands of PNIPAM in pure water below the LCST appear at 1624 and 1562 cm^{-1}, respectively. The single peak of amide I band at 1624 cm^{-1} below the LCST indicates that all the carbonyl groups are hydrogen bonded to water.[65,43] More specifically, C═O group forms hydrogen bonds with two water molecules based on experimental and theoretical studies.[43] It was found that the amide I peak measured above the LCST consist of two Gaussian components 1624 and 1652 cm^{-1}, in which the later band represents the intra- or interchain hydrogen bonds (C═O···H−N).[86] Maeda et al.[86] have observed that about 13% of the C═O groups form intra- or interchain hydrogen bonds (C═O···H−N) above the transition temperature, although the remaining C═O groups still form hydrogen bonds with water.

From a close inspection of Figure 4a−c, we cannot find any new band or significant spectral changes in the amide I and II bands in the presence of buffer. This behavior was observed no matter what the buffer is. With increasing the buffer concentration a binary spectral intensity change due to the transformation of the hydrated C═O (C═O···HOH, 1624 cm^{-1}) to form a hydrogen bond with an N−H group and makes an intra- and interchain cross-linking (C═O···H−N, ∼1652 cm^{-1}). The intensity of the amide II band decreases with increasing the buffer concentration from 0.1 to 0.5 M with no significant shift in frequency. While it is shown gradually shifting from a higher frequency (1562 cm^{-1}) to lower wavenumber with increasing the buffer concentration above 0.5 M. This is also indicative of a binary spectral intensity change, corresponding to the conversion between N−H···H_2O and N−H···O═C hydrogen bonds. Therefore, the addition of buffer causes dehydration of the amide group especially at higher buffer concentrations. This interpretation is strongly supported by the presence of peak with a larger hydrodynamic diameter at higher buffer concentrations (>0.5 M) below the LCST, as shown in the intensity distribution graphs. Consequently, as the cosolvent concentration is increased at a constant temperature, the buffer aqueous solution is gradually becoming a worse "solvent" for the PNIPAM. As a result, the polymer will undergo a coil-to-globule transition at lower temperatures. However, it is reasonable that at buffer concentrations ≤0.5 M the buffer forms hydrogen bonds with a water molecule that is directly H-bonded to the amide groups (Scheme 1), since the d_H

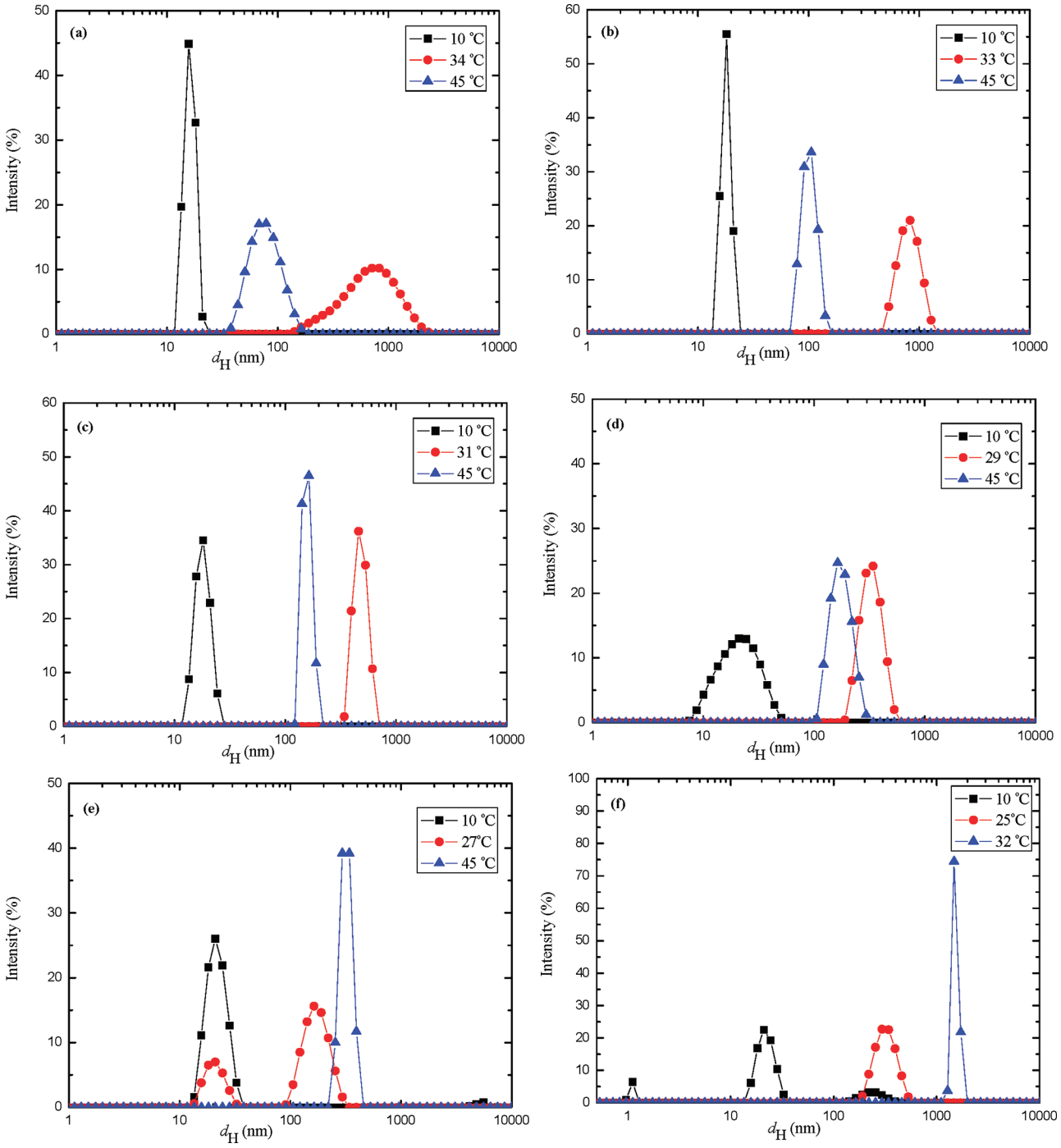

Figure 3. DLS spectra of intensity distribution graph as a typical size distribution in nanometers of PNIPAM in 0.0 M MES (a), 0.1 M MES (b), 0.3 M MES (c), 0.5 M MES (d), 0.7 M MES (e), and 0.9 M MES (f) at various temperatures.

values in PNIPAM buffer solutions are higher than those in pure water below the LCST (Tables 1−3).

To explore whether the amide I and II bands from being hindered by IR bands of water, we studied them in D_2O−buffer solutions (0.0, 0.3, and 0.7 M) at 20 °C, since the δ(O−H) band of water around 1640 cm^{-1} which almost coincides with the amide I band.[32] The main spectral difference caused by the change of H_2O by D_2O in PNIPAM is the amide II band at 1562 cm^{-1}, which moves to ∼1471 cm^{-1} (Figure 4d−f). This is because the amide II contains a contribution from an N−H bend vibration, and this group is deuterated in D_2O.[86] However, the effect of the addition of buffer on the amide I and II bands of PNIAPM in D_2O solutions is similar that in H_2O solutions, except the width of amid I in water is greater than that in D_2O.

The buffers under study have both hydrogen bond donor and acceptor atoms, which can form hydrogen bonds with water. We found that MES, MOPS, and MOPSO in aqueous solution form respectively three, seven, and five H-bonds with water under a periodic boundary condition. Almost of these water molecules are in H-bonded with the sulfonic group,

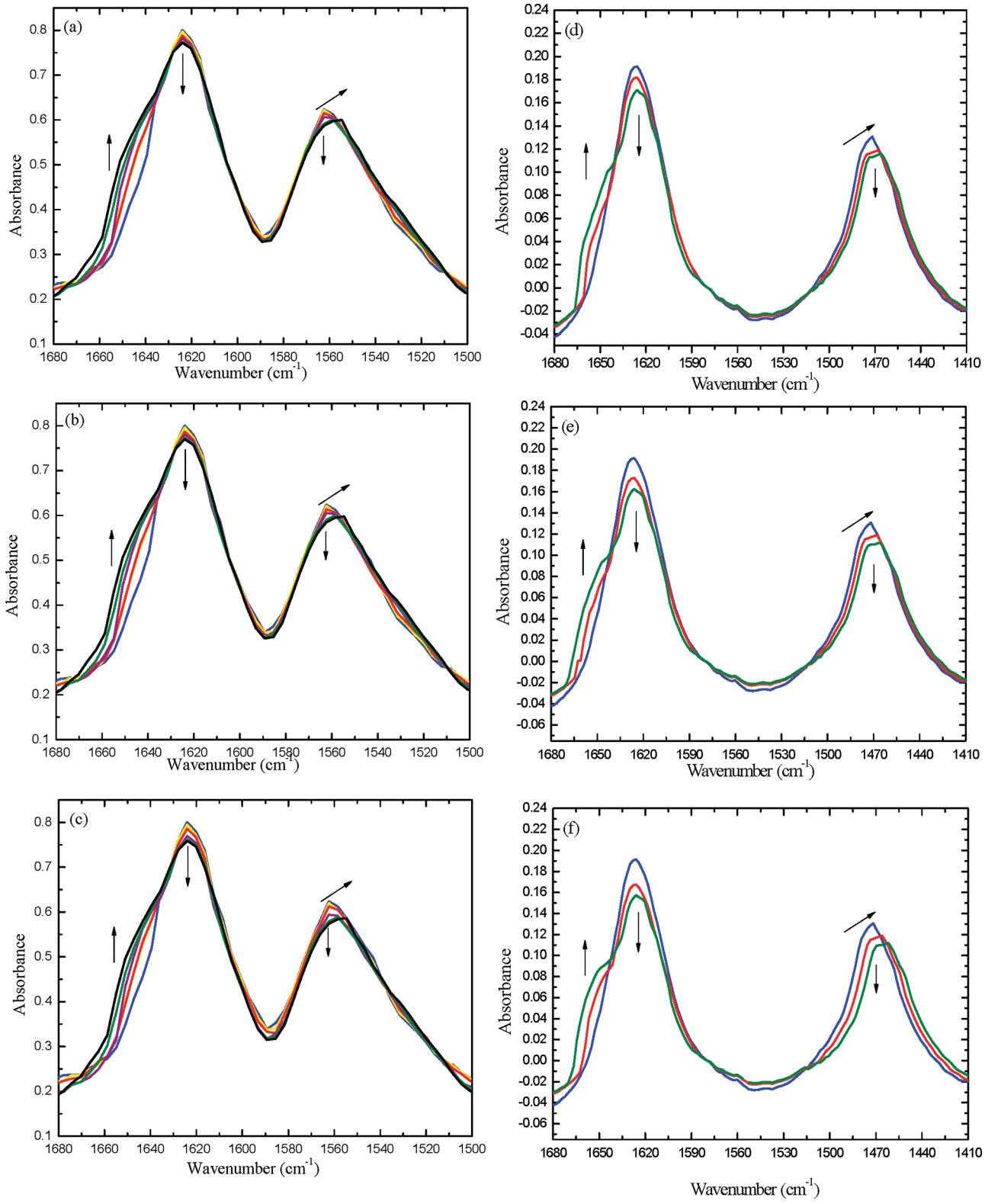

Figure 4. FTIR spectra of PNIPAM in H_2O buffer solutions (a−c) and in D_2O buffer solutions (d−f) of MES (a, d), MOPS (b, e), and MOPSO (c, f) at 20 °C; blue lines (H_2O/D_2O), yellow lines (0.1 M buffer), red lines (0.3 M buffer), purple lines (0.5 M buffer), olive lines (0.7 M buffer), and black lines (0.9 M buffer).

i.e., three, five, and three water molecules form H-bonds with the SO_3^- group of MES, MOPS, and MOPSO, respectively. By using the B3LYP/6-31G method, the total energies obtained in gas phase for MES, MOPS, and MOPSO, e.g., −989.432 62, −1028.695 95, and −1103.882 00 au, respectively, are lower than the corresponding values obtained in aqueous phase,

dx.doi.org/10.1021/ma201790c |*Macromolecules* 2011, 44, 8575–8589

e.g., −989.375 81, −1028.423 77, and −1103.425 82 au for MES, MOPS, and MOPSO, respectively. This result is expected because geometry optimization is carried out by the B3LYP/6-31G method in the gas phase case, but only by classical molecular mechanics in the aqueous solution case. The AMBER functional form for the force field with the bond lengths, bond angles, torsional angles, van der Waals interactions, hydrogen bonds, and electrostatic interactions as the components was used in the molecular simulation. All forces and the total energies of these buffers in aqueous solutions are listed in Table 4. We can see that the contribution of the electrostatic is dominant. The steric energy (bond stretching, angle bending, and torsion deformation) and van der Waals interaction are positive, whereas the electrostatic interaction and hydrogen bond energy are negative. The buffer's affinity to water follows the order MOPS > MES > MOPSO, as seen from and the total energies (Table 4). This order is different from the lowering order of LCST values. The large difference between MOSPO and MOPS in the depression of the LCST effect is quite curious. Their structures are similar, except MOPSO has one more OH group between the zwitterions, as we have mentioned before. This OH group probably interacts with water clusters around the isopropyl groups. Since several studies have reported that the OH groups can interact with water clusters (icebergs or cages) surrounded the hydrophobic isopropyl groups leads to a change in the hydration state of the polymer.[87,88]

From the previous discussion, we see that the influence of the studied buffers on PNIPAM is similar to those observed with protein stabilizers (kosmotropic salts and sugars). Thus, it is suggested that using buffers at high concentrations not only can offer higher buffering capacities but also can provide useful applications regarding proteins.

Scheme 1. Schematic Illustration of Hydrogen Bonds (···) between Amide Group of PNIPAM with Water and MOPS Buffer below the LCST[a]

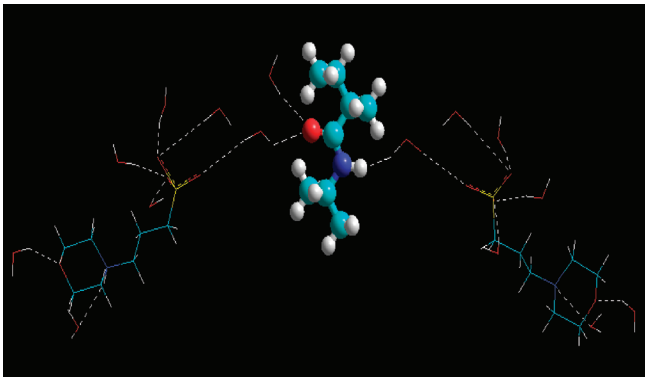

[a] Representation of colors: blue = nitrogen, red = oxygen, gray = hydrogen, and cyan = carbon.

We move now on to investigate the influence of these buffers, especially at high concentrations, on BSA protein for our experimental validation. DLS technique is ideal for studying the critical-thermal denaturation temperature (T_c) of protein; i.e., the temperature corresponds to the beginning of the denaturation process. The d_H values of BSA in 0.05, 0.2, and 1 M buffer (MES, MOPS, or MOPSO) at pH = 7.0, as a function of temperature were detected by DLS measurements (Figure 5). When temperature approached the T_c value, the hydrodynamic size of BSA increased significantly. At this temperature the protein molecules are unfolding and followed by irreversible aggregation of the unfolded molecules, which changes the protein size. Several investigations have been carried out by use of various spectroscopic methods to investigate heat-induced denaturation of BSA, with the following conclusions.[89] Conformational changes of the BSA molecule are reversible in the temperature range of 42−50 °C and irreversible in the temperature range of 52−60 °C. From 60 °C, the unfolding of BSA progresses of the BSA molecule begins. The gel formation results from further unfolding of BSA starts above 70 °C. Figure 5 shows that the T_c value of the native protein in 0.05 M buffer is 55 °C, indicating that BSA is in folded state below 55 °C. The BSA starts to denature with increasing temperature beyond its T_c value. Cooling the protein samples from their respective T_c values to 25 °C does not change the aggregates size. This confirms the irreversible character of BSA denaturation. As we expected, the results presented in Figure 5 show that the thermal stability of BSA increases with increasing buffer concentration. Since, increasing the buffer concentration increased the T_c value of BSA. The T_c values of BSA are 56 and 59 °C for MES, 56 and 62 °C for MOPS, and 56 and 61 °C for MOPSO in 0.2 and 1 M buffer solutions, respectively. From this we can see that the effect of these buffers on the thermal stability of BSA is same at 0.2 M buffer. While at 1 M buffer, the order of increasing the thermal stability of BSA is MOPS > MOPSO > MES. The effect of MOPS in increasing the T_c value, at 1 M, is greater than that of MOPSO, which does not follow as we expected from the PNIPAM results. Probably, MOPSO interacts with other groups of BSA that could participate in destabilizing protein structure (as hereafter inferred from the UV−vis results). It is worthy to compare the stabilization of BSA by these buffers with the former one for TRIS buffer.[85] The T_c values of BSA in 0.05 and 1.0 M TRIS are 55 and 62 °C, respectively.[85] Thus, the stability of BSA in TRIS aqueous solution in the range of 0.05−1.0 M is close to that in MOPS/MOPSO aqueous solution. It was found that TRIS buffer at high concentrations succeeded to suppress the gel formation of BSA solution above 70 °C.[85] In contrast, we found here the studied buffer does not suppress the gel formation of BSA.

The size distribution of BSA aggregates in 1 M buffer (MES, MOPS, or MOPSO) solution at different temperatures is represented in Figure 6. We do not show all the distribution graphs for the sake of clarity of figures. As it can be seen from Figure 6a, there is only one kind of BSA particle size in 1 M MES, before and after the T_c value (59 °C). The particle size is remained constant

Table 4. Contributions to the AMBER Total Energy for the Optimized Buffer in Aqueous Solution[a]

systems	bond	angle	dihedral	vdW	H-bond	electrostatic	total E
MES in water	27.6503	55.7378	3.5275	52.5408	2.9515	−3319.21	−3182.70
MOPS in water	29.7069	69.2757	6.3302	30.8117	−4.7135	−3334.28	−3202.87
MOPSO in water	29.2167	82.0788	7.1077	79.1189	−4.2028	−3327.98	−3134.66

[a] All values in kcal mol^{-1} units.

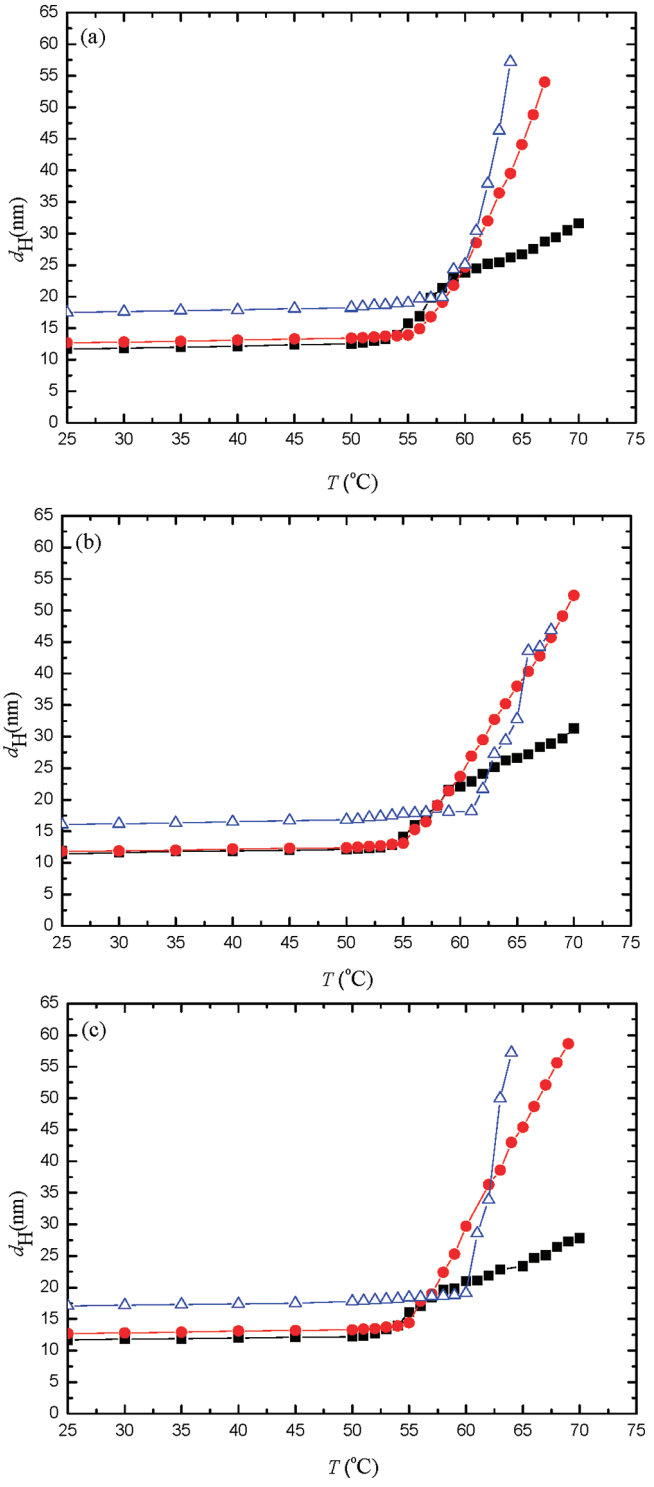

Figure 5. Hydrodynamic diameter (d_H) obtained from the intensity distribution graph as a function of temperature for BSA in 0.05, 0.2, and 1.0 M of MES (a), MOPS (b), or MOPSO (c) as a function of temperature: 0.0 M (■), 0.2 M (●), and 1.0 M (△).

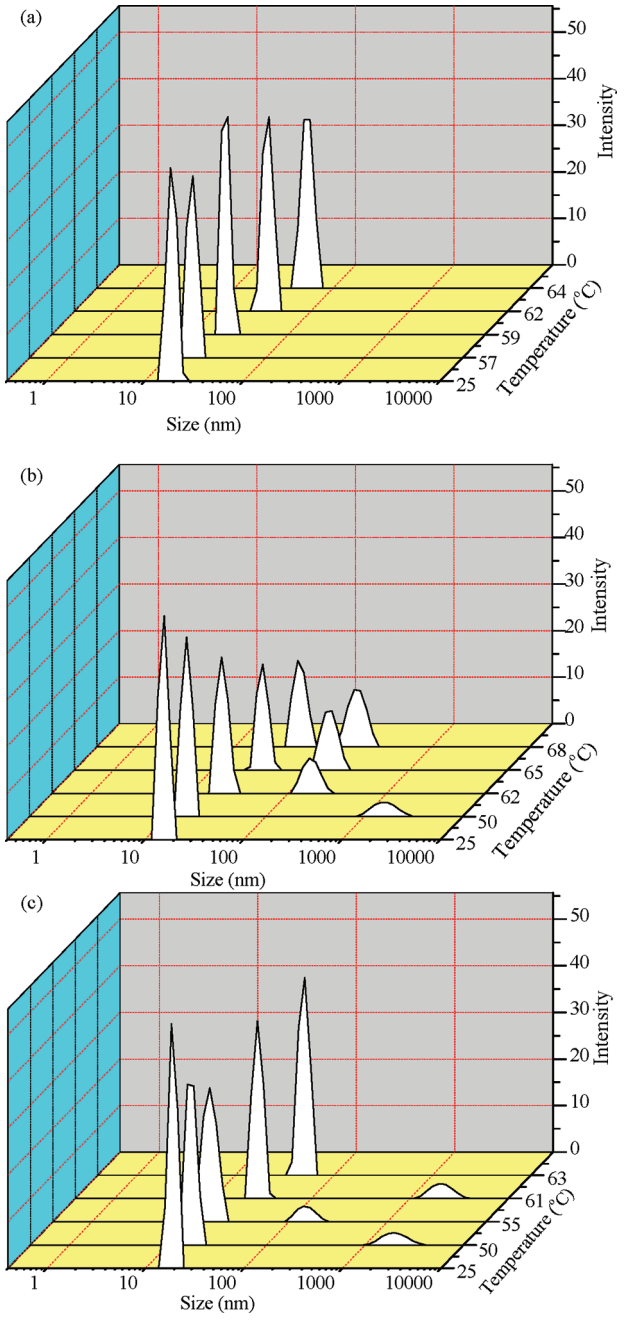

Figure 6. DLS spectra of intensity distribution graph as a typical size distribution in nanometers of BSA in 1.0 M buffer (pH = 7.0): MES (a), MOPS (b), and MOPSO (c) at various temperatures.

in the temperatures from 25 to 58 °C and starts to increase beyond the T_c value. Figure 6b shows that BSA in 1 M MOPS exhibited two peaks starting from 50 to 68 °C. The size of one kind was obtained from native state (more population) of small particles and increased with temperature beyond its T_c value. The size of the aggregates of another kind is large with lower intensity. Two peaks are also observed for BSA in 1 M MOPSO in the temperature range 50−61 °C.

The UV−vis absorbance spectra of BSA, between 200 and 350 nm, in various concentrations of buffer (0.05, 0.2, 0.5, and 1.0 M) at 25 °C are shown in Figure 7. As demonstrated in that figure, proteins absorb UV light with two distinct peaks. The UV absorption of BSA solutions at wavelengths greater than 250 nm, peaking near 280 nm, is principally due to the aromatic side chains of tryptophan, tyrosine, and phenylalanine, listed in order of activity.[74] BSA protein has homologous tryptophan, at position 212, plus a second on at position 134.

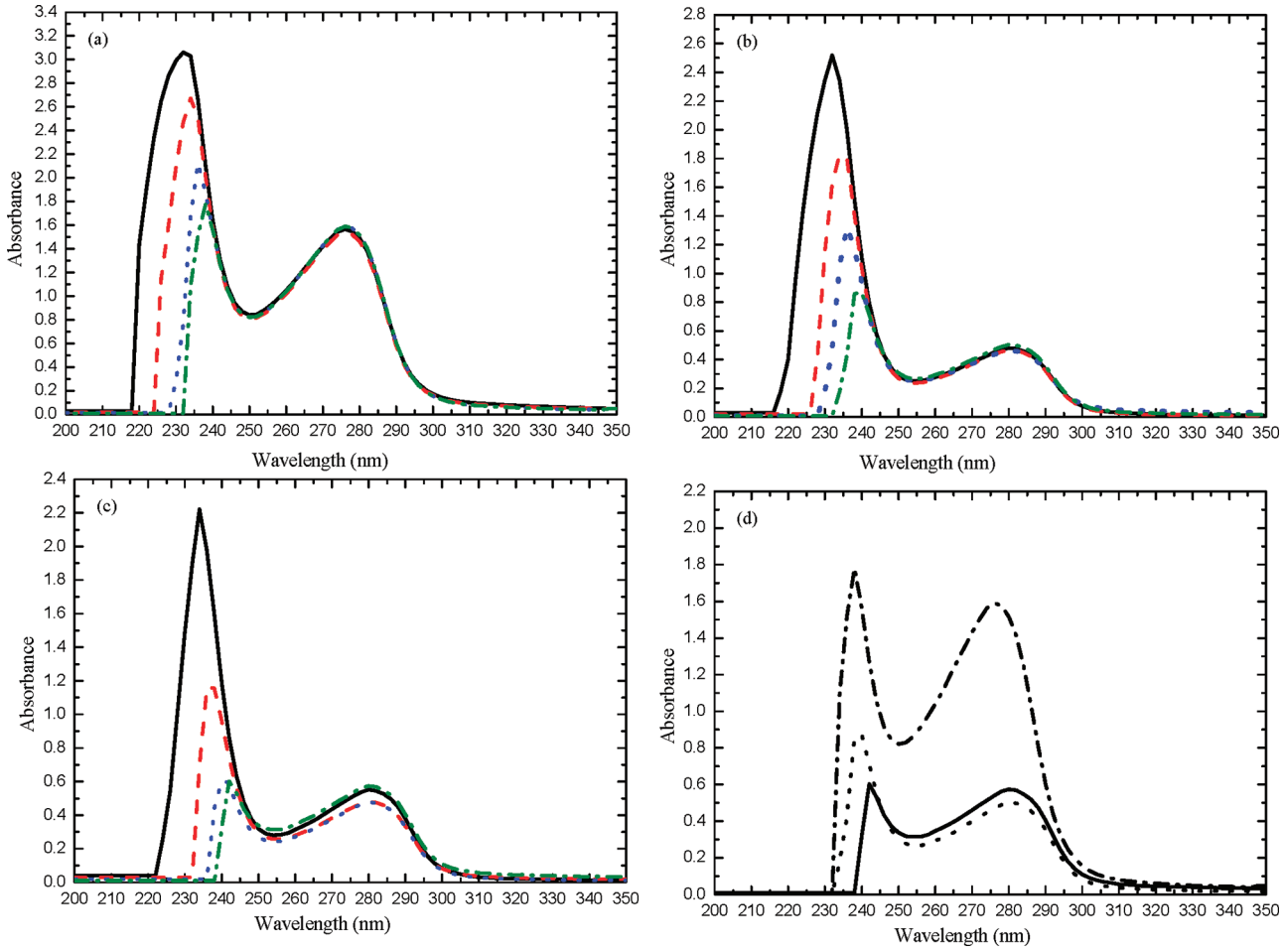

Figure 7. UV−vis spectra of BSA in 0.05, 0.2, 0.5, and 1.0 M buffer (pH = 7.0): MES (a), MOPS (b), and MOPSO (c) at 25 °C; black solid lines (0.05 M), red dashed lines (0.2 M), blue dotted lines (0.5 M), and olive dash-dotted lines (1.0 M). (d) UV−vis spectra of BSA in 1.0 M buffer (pH = 7.0), dash-dotted line (MES), dotted line (MOPS), and solid line (MOPSO) at 25 °C.

In addition, BSA has 20 tyrosine residues and 27 phenylalanine residues. The molar absorptivities, ε_{280nm}, for tryptophan, tyrosine, and phenylalanine are 5540, 1480, and ≈0, respectively. In the UV region below 240 nm, the absorbance of the peptide bond predominates.

Figure 7a−c shows that the BSA peak at higher wavelengths is centered on 276 nm in 0.05 M MES solutions (Figure 7a), while it appears at 280 nm in 0.05 M MOPS (Figure 7b) or MOPSO (Figure 7c) solution. This indicates that the effect of MOPS and MOPSO on the aromatic ring portion of BSA is similar compared to that in MES solutions. The position and intensity of this peak are almost constant for the respective buffer with increasing its concentration in the studied concentration range. The BSA peak at lower wavelength appears at 232 nm in 0.05 M solution of MES or MOPS. This peak shifted to longer wavelengths and became less intense as the buffer concentration is increased, i.e., 234 and 236 nm in 0.2 and 0.5 M solutions (MES or MOPS), respectively. The shifting of this peak is smaller in 1.0 M MES (238 nm) than that in 1.0 M MOPS (240 nm). Also, the peak at lower wavelength is shifted longer wavelengths, and its intensity is decreased with increasing the buffer concentration. The effect of MOPSO buffer on the short-wavelength region is more profound than those of MES and MOPS; the observed shifting in wavelengths are 236, 240, and 242 nm in 0.2, 0.5, and 1.0 M MOPSO, respectively. For the convenience of comparison, the spectra of BSA protein in 1.0 M buffer (MES, MOPS, or MOPSO) are shown in Figure 7d.

The observed red shift at the short wavelength of BSA with increasing the buffer concentration might arise from the disturbance of the microenvironment around the polypeptide backbone. The peptide absorption is due to an $n \rightarrow \pi^*$ transition.[90] The perturbation in this transition region by changes in solvent can cause a red shift with decreasing polarity of the solvent.[90] The shielding of the peptide moieties from the aqueous environments would cause red shifts; i.e., a lower energy is required, and the π^* transition would undergo a red sift accompany with decreasing in absorption. From these spectral changes, it is concluded that peptide moieties are involved in the binding at high-energy sites.

The analysis of the IR spectrum of protein in water solutions is very complicated due to overlapping of amide I band with a broad spectral feature of water. This problem can be avoided by replacing water by heavy water. Figure 8 shows the infrared spectra of BSA protein at 25 °C in 1700−1350 cm^{-1} range in 0.05 and 1.0 M D_2O buffer (MES, MOPS, or MOPSO), at pD = 7.4. The IR spectrum of protein is dominated by bands due to the amide I′ (mainly C═O stretching vibration), amide II (coupling of the N−H bending and C−N stretching modes), amide II′

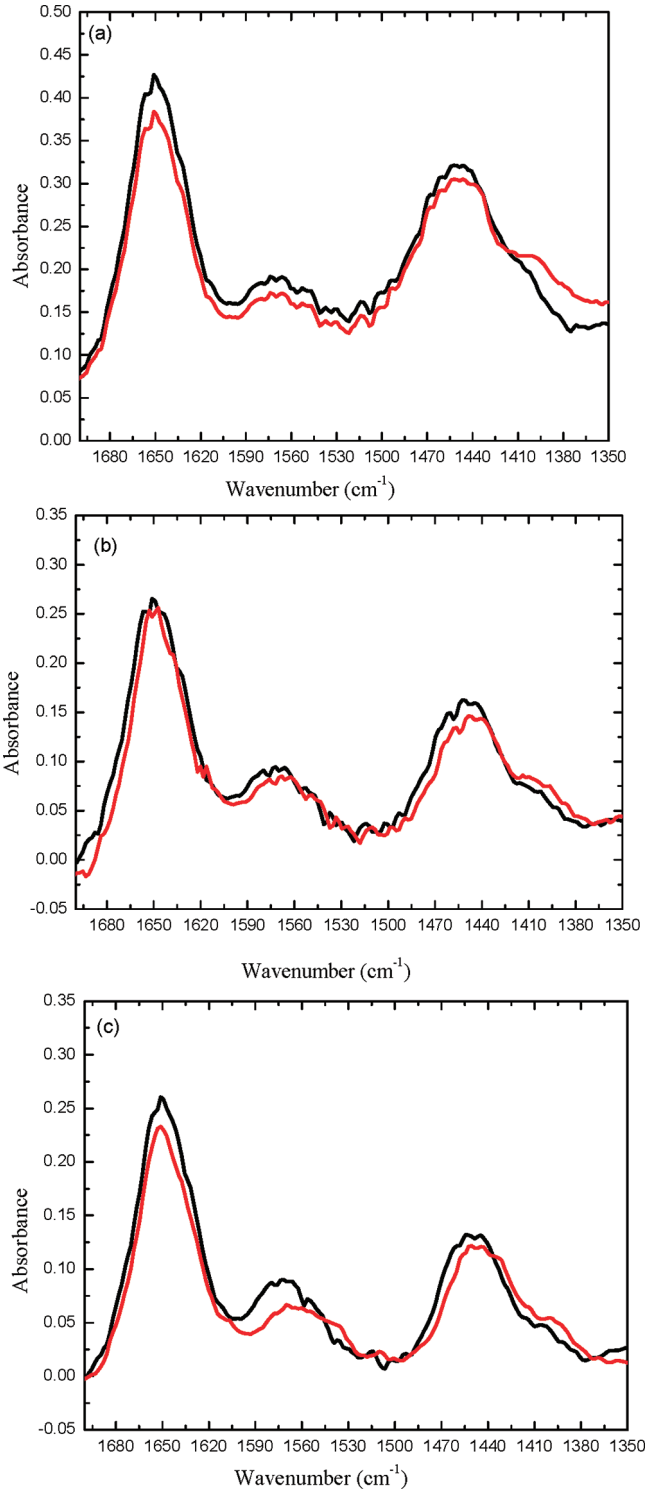

Figure 8. FTIR spectra of PNIPAM in 0.05 and 1.0 M D_2O buffer solutions of MES (a), MOPS (b), and MOPSO (c) at 20 °C; black lines, 0.05 M buffer; red lines, 1.0 M buffer.

(coupling of the N−D bending and C−N stretching modes), and side-chain vibrations.[91] The amide I′, II, and II′ bands of protein at around 1674−1654, 1550, and 1450 cm^{-1}, respectively.[92] The amide II at around 1550 cm^{-1} in H_2O shifts to about 1450 cm^{-1} in D_2O due to the strong sensitivity of the amide II band frequency to the deuteration of the buffer (H/D exchange).[92] The absorption of side chains of protein in solutions in heavy water observed between 1600 and 1500 cm^{-1} such as Glu (near 1570 cm^{-1}), Asp (near 1585 cm^{-1}), Arg (near 1586 cm^{-1}), and Tyr (near 1515 cm^{-1}), respectively.[91]

The amide I′ band of BSA in 0.05 M D_2O buffer (MES, MOPS, or MOPSO) illustrated in Figure 8 appears at 1651 cm^{-1}, and its intensity decreased with increasing the buffer concentrations to 1 M. The amide II′ band is around 1450 cm^{-1} in 0.05 M D_2O buffer (MES, MOPS, or MOPSO). With increasing the MES concentration to 1 M D_2O MES, broadening of the amide II′ band is observed. This band is shifted to lower frequency in 1 M D_2O MOPS or MOPSO. From Figure 8, we can see overlapping of amino acid side-chains spectra with the amide II band in the range of 1600−1500 cm^{-1}, with a maximum intensity at around 1570 cm^{-1} in 0.05 M buffer (MES, MOPS, or MOPSO). The intensity of this peak is decreased with increasing the buffer concentration to 1 M buffer, and its frequency is shifted to lower value in 1 M D_2O MOPS/MOPSO buffer. The IR spectra changes indicate that the studied buffers interact with the peptide moieties of BSA protein, which agree with UV spectra measurements.

4. CONCLUSIONS

The results in this study have shown that when a buffer was introduced into aqueous PNIPAM solution, the buffer was strongly hydrated causing buffering-out of PNIPAM, particularly at higher buffer concentrations. The buffers used in this study are MES, MOPS, and MOPSO, known as morpholine family. From DLS measurements we conclude that the buffers decrease the LCST values of PNIPAM aqueous solutions, by the hydrophobic collapse/aggregation of the PNIPAM. The FTIR measurements showed that the buffers' effect on the LCST values was not through direct binding between the buffer and the polymer. Also, the buffers can bind with water molecules in the first shell of PNIPAM. The LCST values as observed by DLS followed the order MOPSO > MOPS ≈ MES. In fact, these buffers are highly polar compounds and therefore, strongly interact with water molecules. We have also estimated the dipole moment of these buffers in gas phase and in aqueous solution under a periodic boundary condition, by use of DFT and molecular mechanics calculations. It was found that the buffer's affinity to water followed the order MOPS > MES > MOPSO, as deduced from the DFT and molecular simulation under periodic boundary condition. MOPSO significantly decreased the PNIPAM LCST value, in comparing with MOPS buffer. Probably, the extra OH of MOPSO interacts with water clusters around the isopropyl groups leads to a change in the hydration state of PNIPAM. Using buffers at high concentrations can provide useful applications regarding proteins. Thus, we studied the influence of these buffers on the thermal stability of BSA protein using DLS, FTIR, and UV−vis techniques. It was found that these buffers interact with the peptide backbone, leading to net stabilization of BSA. The effects of other buffer families on the conformation of PNIPAM and protein in aqueous solution are currently under our investigation.

■ AUTHOR INFORMATION

Corresponding Author

*Tel +886-2-2737-6626; fax +886-2-2737-6644; e-mail mjlee@mail.ntust.edu.tw.

■ ACKNOWLEDGMENT

The authors gratefully acknowledge the financial support from National Taiwan University of Science and Technology and the National Science Council, Taiwan, through Grant NSC100-2811-E-011-008. M.T. acknowledges postdoc fellowship through this grant. The authors thank Dr. Ho-mu Lin for valuable discussions.

■ REFERENCES

(1) (a) Good, N. E.; Winget, G. D.; Winter, W.; Connolly, T. N.; Izawa, S.; Singh, R. M. M. *Biochemistry* **1966**, *5*, 467–477.
(2) Ferguson, W. J.; Braunschweiger, K. I.; Braunschweiger, W. R.; Smith, J. R.; McCormick, J. J.; Wasmann, C. C.; Jarvis, N. P.; Bell, D. H.; Good, N. E. *Anal. Biochem.* **1980**, *104*, 300–310.
(3) Good, N. E.; Izawa, S. *Methods Enzymol.* **1972**, *24*, 53–68.
(4) Hicks, M.; Gebicki, J. M. *FEBS* **1986**, *199*, 92–94.
(5) Beckman, J. S.; Jun, C.; Ischiropoulos, H.; Crow, J. P. *Methods Enzymol.* **1994**, *233*, 229–240.
(6) Schmidt, K.; Pfeiffer, S.; Mayer, B. *Free Radical Biol. Med.* **1998**, *24*, 859–862.
(7) Welch, K. D.; Davis, T. Z.; Aust, S. D. *Arch. Biochem. Biophys.* **2002**, *397*, 360–369.
(8) Grady, J. K.; Chasteen, N. D.; Harris, D. C. *Anal. Biochem.* **1988**, *173*, 111–115.
(9) Zhao, G.; Chasteen, N. D. *Anal. Biochem.* **2006**, *349*, 262–267.
(10) Kameoka, D.; Masuzaki, E.; Ueda, T.; Imoto, T. *J. Biochem.* **2007**, *142*, 383–391.
(11) Lubas, W. A.; Spiro, R. G. *J. Biol. Chem.* **1988**, *263*, 3990–3998.
(12) Pedrotti, B.; Soffientini, A.; Islam, K. *Cell Motil. Cytoskel.* **1993**, *25*, 234–242.
(13) Kaushal, V.; Barnes, L. D. *Anal. Biochem.* **1986**, *157*, 29l–294.
(14) Peng, L.; Kawagoe, Y.; Hogan, P.; Delmer, D. *Science* **2002**, *295*, 147–150.
(15) Palasz, A. T.; Breña, P. B.; Fuente, J. D.; Gutiérrez-Adán, A. *Theriogenology* **2008**, *70*, 1461–1470.
(16) Edelstein, P. H.; Edelstein, M. A. *J. Clin. Microbiol.* **1993**, *31*, 3329–3330.
(17) Stellwagen, N. C.; Bossi, A.; Gelfi, C.; Righetti, P. G. *Anal. Biochem.* **2000**, *287*, 167–175.
(18) Newman, J. *Acta Crystallogr.* **2004**, *D60*, 610–612.
(19) Fitzgerald, P. M. D.; Wu, J. K.; Toney, J. H. *Biochemistry* **1998**, *37*, 6791–6800.
(20) Knöchel, T. R.; Hennig, M.; Merz, A.; Darimont, B.; Kirschner, K.; Jansonius, J. N. *J. Mol. Biol.* **1996**, *262*, 502–515.
(21) Toney, M. D.; Hohenester, E.; Cowan, S. W.; Jansonius, J. N. *Science* **1993**, *261*, 756–759.
(22) Long, D.; Yang, D. *Biophys. J.* **2009**, *96*, 1482–1488.
(23) Al-Manasir, N.; Zhu, K.; Kjøniksen, A.-L.; Knudsen, K. D.; Karlsson, G.; Nystr øm, B. *J. Phys. Chem. B* **2009**, *113*, 11115–11123.
(24) Zhang, Y.; Furyk, S.; Bergbreiter, D. E.; Cremer, P. S. *J. Am. Chem. Soc.* **2005**, *127*, 14505–14510.
(25) Meersman, F.; Wang, J.; Wu, Y.; Heremans, K. *Macromolecules* **2005**, *38*, 8923–8928.
(26) López-Pérez, P. M.; da Silva, R. M. P.; Pashkuleva, I.; Parra, F.; Reis, R. L.; Roman, J. S. *Langmuir* **2010**, *26*, 5934–5941.
(27) Ono, Y.; Shikata, T. *J. Am. Chem. Soc.* **2006**, *128*, 10030–10031.
(28) Ye, X.; Lu, Y.; Shen, L.; Ding, Y.; Liu, S.; Zhang, G.; Wu, C. *Macromolecules* **2007**, *40*, 4750–4752.
(29) Zhou, K.; Lu, Y.; Li, J.; Shen, L.; Zhang, G.; Xie, Z.; Wu, C. *Macromolecules* **2008**, *41*, 8927–8931.
(30) Sun, B.; Lin, Y.; Wu, P.; Siesler, H. *Macromolecules* **2008**, *41*, 1512–1520.
(31) Ding, Y.; Ye, X.; Zhang, G. *Macromolecules* **2005**, *38*, 904–908.
(32) Sun, S.; Wu, P. *Macromolecules* **2010**, *43*, 9501–9510.
(33) Sun, S.; Hu, J.; Tang, H.; Wu, P. *J. Phys. Chem. B* **2010**, *114*, 9761–9770.
(34) Wu, C.; Zhou, S. *J. Polym. Sci., Part B: Polym. Phys.* **1996**, *34*, 1597–1604.
(35) Freitag, R.; Garret-Flaudy, F. *Langmuir* **2002**, *18*, 3434–3440.
(36) Du, H.; Wickramasinghe, R.; Qian, X. *J. Phys. Chem. B* **2010**, *114*, 16594–16604.
(37) Zhang, Y.; Furyk, S.; Sagle, L. B.; Cho, Y.; Bergbreiter, D. E.; Cremer, P. S. *J. Phys. Chem. C* **2007**, *111*, 8916–8924.
(38) Mukae, K.; Sakurai, M.; Sawamura, S.; Makino, K.; Kim, S.; Ueda, I.; Shirahama, K. *J. Phys. Chem.* **1993**, *97*, 737–741.
(39) Zhu, P. W.; Napper, D. H. *J. Colloid Interface Sci.* **1996**, *177*, 343–352.
(40) Costa, R. O. R.; Freitas, R. F. S. *Polymer* **2002**, *43*, 5879–5885.
(41) Jung, S. C.; Oh, S. Y.; Bae, Y. C. *Polymer* **2009**, *50*, 3370–3377.
(42) Zhu, P.; Napper, D. *Chem. Phys. Lett.* **1996**, *256*, 51–56.
(43) Yamauchi, H.; Maeda, Y. *J. Phys. Chem. B* **2007**, *111*, 12964–12968.
(44) Dalkas, G.; Pagonis, K.; Bokias, G. *Polymer* **2006**, *47*, 243–248.
(45) Pagonis, K.; Bokias, G. *Polym. Int.* **2006**, *55*, 1254–1258.
(46) Pagonis, K.; Bokias, G. *Polym. Bull.* **2007**, *58*, 289–294.
(47) Winnik, F. M.; Ottaviani, M. F.; Bossmann, S. H.; Pan, W.; Garcia-Garibay, M.; Turro, N. J. *Macromolecules* **1993**, *26*, 4577–4585.
(48) Zhang, X. Z.; Chu, C. C. *Colloid Polym. Sci.* **2004**, *282*, 589–595.
(49) Winnik, F. M.; Ringsdorf, H.; Venzmer, J. *Macromolecules* **1990**, *23*, 2415–2416.
(50) Schild, H. G.; Muthukumar, M.; Tirrell, D. A. *Macromolecules* **1991**, *24*, 948–952.
(51) Winnik, F. M.; Ottaviani, M. F.; Bossmann, S. H.; Garcia-Garibay, M.; Turro, N. J. *Macromolecules* **1992**, *25*, 6007–6017.
(52) Zhang, G.; Wu, C. *Phys. Rev. Lett.* **2001**, *86*, 822–825.
(53) Zhang, G.; Wu, C. *J. Am. Chem. Soc.* **2001**, *123*, 1376–1380.
(54) Shimizu, S.; Kurita, K.; Furusaka, M. *Appl. Phys. A: Mater. Sci. Process.* **2002**, *74*, 389–396.
(55) Tao, C.; Young, T. *Polymer* **2005**, *46*, 10077–10084.
(56) Tanaka, F.; Koga, T.; Winnik, F. *Phys. Rev. Lett.* **2008**, *101*, 028302[1−4].
(57) Chen, J.-H.; Chen, H.-H.; Chang, Y.-X.; Chuang, P.-Y.; Hong, P.-D. *J. Appl. Polym. Sci.* **2008**, *107*, 2732–2742.
(58) Tanaka, F.; Koga, T.; Kojima, H.; Winnik, F. M. *Macromolecules* **2009**, *42*, 1321–1130.
(59) Pang, J.; Yang, H.; Ma, J.; Cheng, R. *J. Phys. Chem. B* **2010**, *114*, 8652–8658.
(60) Tiktopulo, E. I.; Uversky, V. N.; Lushchik, V. B.; Klenin, S. I.; Bychkova, V. E.; Ptitsyn, O. B. *Macromolecules* **1995**, *28*, 7519–7524.
(61) Lee, L.-T.; Cabane, B. *Macromolecules* **1997**, *30*, 6559–6566.
(62) Mylonas, Y.; Staikos, G. *Langmuir* **1999**, *15*, 7172–7175.
(63) Zhu, P. W.; Napper, D. H. *Langmuir* **1996**, *12*, 5992–5998.
(64) Walter, R.; Ricka, J.; Quellet, C. H.; Nuffenger, R.; Binkert, T. H. *Macromolecules* **1996**, *29*, 4019–4028.
(65) Sagle, B. L.; Zhang, Y.; Litosh, V. A.; Chen, X.; Cho, Y.; Cremer, P. S. *J. Am. Chem. Soc.* **2009**, *131*, 9304–9310.
(66) Shpigelman, A.; Paz, Y.; Ramon, O.; Livney, Y. D. *Colloid Polym. Sci.* **2011**, *289*, 281–290.
(67) Reddy, P. M.; Venkatesu, P. *J. Phys. Chem. B* **2011**, *115*, 4752–4757.
(68) Wei, H.; Zhang, X.; Cheng, C.; Cheng, S. X.; Zhuo, R. X. *Biomaterials* **2007**, *28*, 99–107.
(69) Kono, K.; Henmi, A.; Yamashita, H.; Hayashi, H.; Takagishi, T. *J. Controlled Release* **1999**, *59*, 63–75.
(70) Akiyama, Y.; Kikuchi, A.; Yamato, M.; Okano, T. *Langmuir* **2004**, *20*, 5506–5511.
(71) Suzuki, D.; Kawaguchi, H. *Colloid Polym. Sci.* **2006**, *284*, 1443–1451.
(72) Kokufuta, E.; Zhang, Y. Q.; Tanaka, T. *Nature* **1991**, *351*, 302–304.
(73) Bergbreiter, D. E.; Case, B. L.; Liu, Y. S.; Caraway, J. W. *Macromolecules* **1998**, *31*, 6053–6062.
(74) Peters, T. *All about Albumin*; Academic Press: San Diego, CA, 1996.

(75) HyperChem 8.0.7, Hypercube, Inc., Gainesville, FL.
(76) Jorgensen, W. L.; Chandasekhar, J.; Madura, J. D.; Impey, R. W.; Klein, M. L. *J. Chem. Phys.* **1983**, *79*, 926–935.
(77) Collins, K. D.; Washabaugh, M. W. *Q. Rev. Biophys.* **1985**, *18*, 323–422.
(78) Xie, G.; Timasheff, S. N. *Biophys. Chem.* **1997**, *64*, 25–43.
(79) Xie, G.; Timasheff, S. N. *Protein Sci.* **1997**, *6*, 211–221.
(80) Taha, M.; Lee, M. J. *J. Chem. Eng. Data* **2011**, DOI: 10.1021/je200244p.
(81) Taha, M.; Lee, M. J. *J. Chem. Thermodyn.* **2011**, *43*, 1723–1730.
(82) Kirkwood, J. G. *J. Chem. Phys.* **1934**, *2*, 351–361.
(83) Neuberger, A. *Proc. R. Soc. London A* **1937**, *158*, 68–96.
(84) Robinson, R. A.; Stokes, R. H. *Electrolyte Solutions*; Dover: Mineola, NY, 2002.
(85) Taha, M.; Lee, M. J. *Phys. Chem. Chem. Phys.* **2010**, *12*, 12840–12850.
(86) Maeda, Y.; Nakamura, T.; Ikeda, I. *Macromolecules* **2001**, *34*, 8246–8251.
(87) Shpigelman, A.; Portnaya, I.; Ramon, O.; Livney, Y. D. *J. Polym Sci., Part B: Polym. Phys.* **2008**, *46*, 2307–2318.
(88) Kato, N.; Sakai, Y.; Takahashi, F. *Bull. Chem. Soc. Jpn.* **2001**, *74*, 2025–2029.
(89) Murayama, K.; Tomida, M. *Biochemistry* **2004**, *43*, 11526–11532.
(90) Poet, H.; Steinhardt, J. *Biochemistry* **1968**, *7*, 1348–1346.
(91) Murayama, K.; Tomida, M. *Biochemistry* **2004**, *43*, 11526–11532.
(92) Jung, C. *Anal. Bioanal. Chem.* **2008**, *392*, 1031–1058.